JOURNAL OF GUIDANCE, CONTROL, AND DYNAMICS
Vol. 19, No. 5, September–October 1996

Moving Mass Trim Control for Aerospace Vehicles

Rush D. Robinett III,* Beverly R. Sturgis,† and Shawn A. Kerr‡
Sandia National Laboratories, Albuquerque, New Mexico 87185

A moving mass trim controller is proposed to increase the accuracy of axisymmetric, ballistic vehicles. The moving mass trim controller differs from other moving mass schemes because it generates an angle of attack directly from the mass motion. The nonlinear equations of motion for a ballistic vehicle with one moving point mass are derived and provide the basis for a detailed simulation model. The nonlinear equations are linearized to produce a set of linear, time-varying autopilot equations. These autopilot equations are analyzed and used to develop theoretical design tools for the creation of moving mass trim controllers for both fast and slow spinning vehicles. A fast spinning moving mass trim controller is designed for a generic artillery rocket that uses principal axis misalignment to generate a trim angle of attack. A slow spinning moving mass trim controller is designed for a generic re-entry vehicle that generates a trim angle of attack with a center of mass offset and aerodynamic drag. The performance of both moving mass trim controllers are evaluated with the detailed simulation.

Introduction

OVER the years, techniques for controlling the flight characteristics of missiles and re-entry vehicles (RV) have gravitated to systems that deliver relatively large amounts of control authority. For certain missions, such as an air-to-air missile or an RV designed to evade defenses, a large lateral acceleration capability was required. The technologies used to perform these missions ranged from actuated canards, elevons, and flaps to jet interaction, thrust vector control, and a variety of other techniques.[1] Because of the mission requirements for large maneuvers, systems that provided modest amounts of control capability were of little or no value. However, a new mission for accurate artillery rockets and RVs that utilize existing assets has prompted a renewed interest in simpler control techniques that produce small maneuvers.

One such control technology is moving mass control. This technique has previously been evaluated in conjunction with other control methods such as the moving mass roll control of an aerodynamically asymmetric RV.[2,3] A more direct application of moving mass control technology is the moving mass trim controller (MMTC). The MMTC generates a trim angle of attack (AOA) on an axisymmetric, ballistic vehicle directly from the motion of the mass. It is a novel, lightweight, low-cost retrofit to spinning ballistic vehicles that require modest flight-path corrections to obtain increased accuracy.

Over 10 years ago, initial studies of the MMTC were performed by Regan and Kavetsky[4] at the U.S. Naval Systems Warfare Center. Regan and his co-workers devised a single-shot MMTC that would provide modest range corrections near the target. At Sandia National Laboratories (SNL), the MMTC was an outgrowth of the deconing device test (DDT) described by White and Robinett.[5] The DDT provided an initial glimpse of the effects of principal axis misalignment (PAM), roll rate, and center of mass offset. The MMTCs developed at SNL address the issue of roll rate, static margin (SM), PAM, and center of mass offset. The trim AOA for a fast spinning vehicle is generated by a PAM, whereas a slow spinning vehicle with a small SM relies on a center of mass offset to create a trim AOA resulting from aerodynamic drag. This paper derives the general nonlinear equations of motion for a one-moving mass system, the general linear, time-varying autopilot equations, and theoretical design tools that are used to develop conceptual hardware designs for a generic artillery rocket and a generic RV.

Received July 18, 1995; revision received April 15, 1996; accepted for publication April 29, 1996.

*Distinguished Member, Technical Staff, Threat and Countermeasures Development and Evaluation Department. Senior Member AIAA.

†Distinguished Member, Technical Staff, Advanced Concepts and Engineering Systems Analysis Department. Member AIAA.

‡Senior Member, Technical Staff, Advanced Concepts and Engineering Systems Analysis Department. Member AIAA.

Equations of Motion

The system under consideration is shown in Fig. 1. Rigid body B of mass m_B and moving point mass P of mass m_P combine to form system S of mass m_S, where $m_S = m_B + m_P$. Points of interest are B^*, the mass center of B, and S^*, the mass center of S. Coordinate frames are the Earth-centered inertial frame I, the local geodetic frame G made up of north, east, and down unit vectors (denoted as $\bar{g}_1, \bar{g}_2, \bar{g}_3$), the body-fixed frame B (unit vectors $\bar{b}_1, \bar{b}_2, \bar{b}_3$), and the nonrolling frame N (unit vectors $\bar{n}_1, \bar{n}_2, \bar{n}_3$), which pitches and yaws but does not roll with B (see Fig. 1). Pitch, yaw, and roll are defined as a sequence of rotations as follows. After initial alignment of the G and B frames, Euler angle rotations are performed in the following order: 1) yaw (angle ψ) about the $\bar{b}_3$ unit vector, 2) pitch (angle θ) about the new location of the $\bar{b}_2$ unit vector, and 3) roll (angle ϕ) about the final location of the $\bar{b}_1$ unit vector.

The mass may move in all three directions in the body, but its position, velocity, and acceleration in the B frame are controlled using third-order actuator transfer functions in each direction. Therefore, the system is treated as having six degrees of freedom (6 DOF). This approach is used for conceptual studies only. Once an actuator is sized, an 8-DOF simulation with force interaction between the body and actuator is implemented since the axial position of the mass is fixed. The examples in the following sections utilize an actuator force that is equivalent to the theoretical mass acceleration.

Rolling Frame Equations of Motion

Equations of motion expressed in the B frame were derived using two methods. The first method uses Newton's second law and the results are given in this section. Newton's second law is applied to S^* to derive the translational equations and the applied moments about S^* are equated to the time derivative in the inertial frame of the inertial angular momentum of S for S^* to derive the rotational

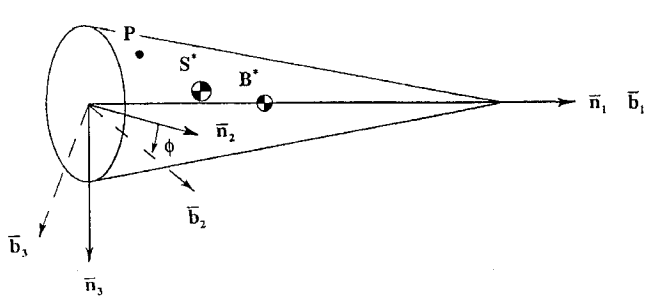

Fig. 1 Ballistic vehicle with one moving point mass.

equations. Kane's method[6] was used as an independent check to verify the equations derived in this section.

The inertial angular velocity of B and the inertial velocity of B^* are defined as

$$ {}^I\omega^B = \omega_1\bar{b}_1 + \omega_2\bar{b}_2 + \omega_3\bar{b}_3 \tag{1} $$

$$ {}^I\nu^{B^*} = \nu_1\bar{b}_1 + \nu_2\bar{b}_2 + \nu_3\bar{b}_3 \tag{2} $$

The mass ratio μ is defined as

$$ \mu = m_p/m_s \tag{3} $$

The position vector from B^* to P is given by

$$ \boldsymbol{p} = p_1\bar{b}_1 + p_2\bar{b}_2 + p_3\bar{b}_3 \tag{4} $$

and the inertial velocity of S^* is given by

$$ {}^I\nu^{S^*} = {}^I\nu^{B^*} + \mu(\dot{\boldsymbol{p}} + {}^I\omega^B \times \boldsymbol{p}) \tag{5} $$

The aerodynamic force is defined as

$$ \boldsymbol{F}_{\text{aero}} = F_1\bar{b}_1 + F_2\bar{b}_2 + F_3\bar{b}_3 \tag{6} $$

and the force resulting from gravity is given by

$$ \boldsymbol{F}_{\text{grav}} = m_s g\left({}^GX_{31}^B\bar{b}_1 + {}^GX_{32}^B\bar{b}_2 + {}^GX_{33}^B\bar{b}_3\right) \tag{7} $$

where g is the gravitational acceleration and ${}^GX^B$ is the direction cosine matrix relating the B frame to the G frame. The three elements of interest for the yaw, pitch, and roll sequence described previously are

$$ \left({}^GX_{31}^B, {}^GX_{32}^B, {}^GX_{33}^B\right) = (-\sin\theta, \cos\theta\sin\phi, \cos\theta\cos\phi) \tag{8} $$

The torque about B^* from aerodynamic forces is defined as

$$ \boldsymbol{T}_{B^*} = T_1\bar{b}_1 + T_2\bar{b}_2 + T_3\bar{b}_3 \tag{9} $$

which results in a moment about S^* of

$$ \sum M_{s^*} = T_{B^*} - \mu\boldsymbol{p} \times \boldsymbol{F}_{\text{aero}} \tag{10} $$

The inertial angular momentum of S for S^* is given by

$$ {}^I\boldsymbol{H}^{s/s^*} = \bar{\boldsymbol{I}}^{B/B^*} \cdot {}^I\omega^B + \mu m_B\boldsymbol{p} \times \left({}^I\nu^P - {}^I\nu^{B^*}\right) \tag{11} $$

where the inertia dyadic of B for B^* and for B frame unit vectors is defined as

$$ \begin{aligned} \bar{\boldsymbol{I}}^{B/B^*} &= I_{11}\bar{b}_1\bar{b}_1 + I_{12}(\bar{b}_1\bar{b}_2 + \bar{b}_2\bar{b}_1) + I_{13}(\bar{b}_1\bar{b}_3 + \bar{b}_3\bar{b}_1) \\ &\quad + I_{22}\bar{b}_2\bar{b}_2 + I_{23}(\bar{b}_2\bar{b}_3 + \bar{b}_3\bar{b}_2) + I_{33}\bar{b}_3\bar{b}_3 \end{aligned} \tag{12} $$

From

$$ \sum \boldsymbol{F}_{S^*} = m_s^I\boldsymbol{a}^{S^*} \qquad \text{and} \qquad \frac{{}^I\mathrm{d}}{\mathrm{d}t}\left({}^I\boldsymbol{H}^{s/s^*}\right) = \sum \boldsymbol{M}_{s^*} $$

the following vector equations of motion are obtained:

$$ \begin{aligned} &{}^I\dot{\nu}^{B^*} + \mu(\ddot{\boldsymbol{p}} + {}^I\dot{\omega}^B \times \boldsymbol{p} + {}^I\omega^B \times \dot{\boldsymbol{p}}) + {}^I\omega^B \\ &\quad \times \left[{}^I\nu^{B^*} + \mu(\dot{\boldsymbol{p}} + {}^I\omega^B \times p)\right] = (1/m_s)(\boldsymbol{F}_{\text{aero}} + \boldsymbol{F}_{\text{grav}}) \end{aligned} \tag{13} $$

$$ \begin{aligned} &\bar{\boldsymbol{I}}^{B/B^*} \cdot {}^I\dot{\omega}^B + \mu m_B\left[\dot{\boldsymbol{p}} \times \left({}^I\nu^P - {}^I\nu^{B^*}\right) + \boldsymbol{p} \times \left({}^I\dot{\nu}^P - {}^I\dot{\nu}^{B^*}\right)\right] \\ &\quad + {}^I\omega^B \times \left[\bar{\boldsymbol{I}}^{B/B^*} \cdot {}^I\omega^B + \mu m_B\boldsymbol{p} \times \left({}^I\nu^P - {}^I\nu^{B^*}\right)\right] \\ &\quad = \boldsymbol{T}_{B^*} - \mu\boldsymbol{p} \times \boldsymbol{F}_{\text{aero}} \end{aligned} \tag{14} $$

Nonrolling Frame Equations of Motion

It is desirable to write guidance algorithms using the equations of motion for the nonrolling frame. Using the same approach as the first method yields the following matrix equations of motion after expanding the prior vector equations with respect to the nonrolling frame:

$$ \begin{aligned} &(\dot{\nu}^N) + \mu[\tilde{p}]({}^I\dot{\omega}^N) = -\mu(\ddot{p}^N) + \left[2\mu[{}^I\tilde{\omega}^N] + (m_B/m_s)[\dot{\tilde{\phi}}]\right](\dot{p}^N) \\ &\quad + [{}^I\tilde{\omega}^N](\nu^N) + [\omega^2](p^N) + (1/m_s)[(\boldsymbol{F}_{\text{aero}}) + (\boldsymbol{F}_{\text{grav}})] \end{aligned} \tag{15} $$

$$ \begin{aligned} &[\bar{J}]({}^I\dot{\omega}^N) = [{}^I\tilde{\omega}^N][\bar{J}]({}^I\omega^N) + (\phi^2) + 2\mu m_B[\omega p](\dot{p}^N) \\ &\quad + \mu m_B[\tilde{p}](\ddot{p}^N) + (\boldsymbol{T}_{B^*}) + \mu[\tilde{p}](\boldsymbol{F}_{\text{aero}}) \end{aligned} \tag{16} $$

where

$$ [\tilde{p}] = \begin{bmatrix} 0 & p_{n3} & -p_{n2} \\ -p_{n3} & 0 & p_{n1} \\ p_{n2} & -p_{n1} & 0 \end{bmatrix} \qquad [{}^I\tilde{\omega}^N] = \begin{bmatrix} 0 & \omega_{INn3} & -\omega_{INn2} \\ -\omega_{INn3} & 0 & \omega_{INn1} \\ \omega_{INn2} & -\omega_{INn1} & 0 \end{bmatrix} \qquad [\dot{\tilde{\phi}}] = \begin{bmatrix} 0 & 0 & 0 \\ 0 & 0 & -\dot{\phi} \\ 0 & \dot{\phi} & 0 \end{bmatrix} $$

$$ [\omega^2] = \begin{bmatrix} \mu\left(\omega_{INn2}^2 + \omega_{INn3}^2\right) & (-\mu\omega_{INn1} + (m_B/m_s)\dot{\phi})\omega_{INn2} & (-\mu\omega_{INn1} + (m_B/m_s)\dot{\phi})\omega_{INn3} \\ -\mu\omega_{INn1}\omega_{INn2} & \left(\mu\left(\omega_{INn1}^2 + \omega_{INn3}^2\right) - (m_B/m_s)\dot{\phi}\omega_{INn1}\right) & (-\mu\omega_{INn2}\omega_{INn3} - (m_B/m_s)\ddot{\phi}) \\ -\mu\omega_{INn1}\omega_{INn3} & (-\mu\omega_{INn2}\omega_{INn3} + (m_B/m_s)\ddot{\phi}) & \left(\mu\left(\omega_{INn1}^2 + \omega_{INn2}^2\right) - (m_B/m_s)\dot{\phi}\omega_{INn1}\right) \end{bmatrix} $$

$$ (\boldsymbol{F}_{\text{grav}}) = m_s g\left({}^GX_{31}^N, {}^GX_{32}^N, {}^GX_{33}^N\right) $$

$$ [\bar{J}] = \begin{bmatrix} \left(J_{11} + \mu m_B\left(p_{n2}^2 + p_{n3}^2\right)\right) & (J_{12} - \mu m_B p_{n1}p_{n2}) & (J_{13} - \mu m_B p_{n1}p_{n3}) \\ (J_{12} - \mu m_B p_{n1}p_{n2}) & \left(J_{22} + \mu m_B\left(p_{n1}^2 + p_{n3}^2\right)\right) & (J_{23} - \mu m_B p_{n2}p_{n3}) \\ (J_{13} - \mu m_B p_{n1}p_{n3}) & (J_{23} - \mu m_B p_{n2}p_{n3}) & \left(J_{33} + \mu m_B\left(p_{n1}^2 + p_{n2}^2\right)\right) \end{bmatrix} $$

$$ (\phi^2) = \begin{pmatrix} -J_{11}\ddot{\phi} \\ -J_{12}\ddot{\phi} + (2(J_{13}\omega_{INn1} + J_{23}\omega_{INn2}) + (J_{33} - J_{22} - J_{11})\omega_{INn3})\dot{\phi} + J_{13}\dot{\phi}^2 \\ -J_{13}\ddot{\phi} - (2(J_{12}\omega_{INn1} + J_{23}\omega_{INn3}) + (J_{33} + J_{11} - J_{22})\omega_{INn2})\dot{\phi} - J_{12}\dot{\phi}^2 \end{pmatrix} $$

$$ [\omega p] = \begin{bmatrix} (\omega_{INn2}p_{n2} + \omega_{INn3}p_{n3}) & -\omega_{INn1}p_{n2} & -\omega_{INn1}p_{n3} \\ -\omega_{INn2}p_{n1} & (\omega_{INn1}p_{n1} + \omega_{INn3}p_{n3}) & -\omega_{INn2}p_{n3} \\ -\omega_{INn3}p_{n1} & -\omega_{INn3}p_{n2} & (\omega_{INn1}p_{n1} + \omega_{INn2}p_{n2}) \end{bmatrix} $$

Definitions of entities different from those defined in the rolling frame equations follow. The inertial angular velocity of N is

$$ {}^{I}\omega^{N} = \omega_{INn1}\bar{n}_1 + \omega_{INn2}\bar{n}_2 + \omega_{INn3}\bar{n}_3 \tag{17} $$

The inertial velocity of B^* is

$$ {}^{I}\boldsymbol{\nu}^{B^*} = \nu_{n1}\bar{n}_1 + \nu_{n2}\bar{n}_2 + \nu_{n3}\bar{n}_3 \tag{18} $$

The aerodynamic force is given by

$$ \boldsymbol{F}_{\text{aero}} = F_{n1}\bar{n}_1 + F_{n2}\bar{n}_2 + F_{n3}\bar{n}_3 \tag{19} $$

The moment from this force about B^* is

$$ \boldsymbol{T}_{B^*} = T_{n1}\bar{n}_1 + T_{n2}\bar{n}_2 + T_{n3}\bar{n}_3 \tag{20} $$

The inertia dyadic of B for B^* and for N frame unit vectors is given by

$$ \bar{I}^{B/B^*} = J_{11}\bar{n}_1\bar{n}_1 + J_{12}(\bar{n}_1\bar{n}_2 + \bar{n}_2\bar{n}_1) + J_{13}(\bar{n}_1\bar{n}_3 + \bar{n}_3\bar{n}_1) + J_{22}\bar{n}_2\bar{n}_2 + J_{23}(\bar{n}_2\bar{n}_3 + \bar{n}_3\bar{n}_2) + J_{33}\bar{n}_3\bar{n}_3 \tag{21} $$

where

$$ J_{11} = I_{11} \qquad J_{12} = I_{12}\cos\phi - I_{13}\sin\phi $$

$$ J_{13} = I_{12}\sin\phi + I_{13}\cos\phi $$

$$ J_{22} = I_{22}\cos^2\phi + I_{33}\sin^2\phi - 2I_{23}\sin\phi\cos\phi $$

$$ J_{23} = (I_{22} - I_{33})\sin\phi\cos\phi + I_{23}(\cos^2\phi - \sin^2\phi) $$

$$ J_{33} = I_{22}\sin^2\phi + I_{33}\cos^2\phi + 2I_{23}\sin\phi\cos\phi $$

Elements of the direction cosine matrix relating the N frame to the G frame appearing in Eqs. (15) are

$$ \left({}^{G}X^{N}_{31}, {}^{G}X^{N}_{32}, {}^{G}X^{N}_{33}\right) = (-\sin\theta, 0, \cos\theta) \tag{22} $$

Autopilot Equations

The autopilot equations are a set of mathematical relationships that relate the AOA and angle of sideslip in the nonrolling frame to the mass motion in the body-fixed frame. In this manner, the guidance commands can be directly related to the actuator commands. The autopilot equations are obtained by linearizing the nonrolling equations of motion [Eqs. (15) and (16)] that were derived in the preceding section. The result of the linearizing procedure is a set of linear, time-varying equations that describe nonrolling AOA and angle of sideslip of the ballistic vehicle.

The linearization procedure follows Ref. 7 and begins with several simplifying assumptions:

1) The effects of gravity are negligible.

2) The vehicle experiences only small angular perturbations ($\alpha, \beta \ll 1$ rad and ω_{INn2}, ω_{INn3}, v_{n2}, and v_{n3} are small perturbation quantities).

3) The moment of inertia tensor is symmetric with $I = J_{22} = J_{33}$ and $I_{xx} = J_{11}$.

4) The mass only moves radially ($p_{n1} = \text{const}$ and $\dot{p}_{n1} = \ddot{p}_{n1} = 0$) and $m_p/m_s \ll 1$.

5) The nonrolling roll rate is constant ($\dot{\omega}_{INn1} = 0$) and equal to zero, and $\ddot{\phi}$ is small (this will be justified later).

6) The vehicle has linear aerodynamics and retains basic aerodynamic symmetry with respect to the longitudinal axis, which implies that aerodynamic asymmetries are small ($|C_{m_0}/C_{m_\alpha}|$, $|C_{n_0}/C_{m_\alpha}| \ll 1$).

Using assumptions 1, 2, and 5 and neglecting nonlinear terms, the translational equations of motion become

$$ F_{n1} = m_s\dot{v}_{n1} \tag{23} $$

$$ F_{n2} = m_s(\dot{v}_{n2} + \omega_{INn3}v_{n1}) + m_B\dot{\phi}\dot{p}_{n3} \tag{24} $$

$$ F_{n3} = m_s(\dot{v}_{n3} - \omega_{INn2}v_{n1}) - m_B\dot{\phi}\dot{p}_{n2} \tag{25} $$

Assumptions 3–5 lead to the following transverse angular rate equations:

$$ M'_{n2} = I'\dot{\omega}_{INn2} + I_{xx}\dot{\phi}\omega_{INn3} - \mu m_B p_{n1}\ddot{p}_{n3} = T_{n2} + \mu p_{n1}F_{n3} - \mu p_{n3}F_{n1} \tag{26} $$

$$ M'_{n3} = I'\dot{\omega}_{INn3} - I_{xx}\dot{\phi}\omega_{INn2} + \mu m_B p_{n1}\ddot{p}_{n2} = T_{n3} - \mu p_{n1}F_{n2} - \mu p_{n2}F_{n1} \tag{27} $$

where

$$ I' = I + \mu m_B p_{n1}^2 $$

At this point, the nonrolling AOA and angle of sideslip are defined as $\alpha = \tan^{-1}(v_{n3}/v_{n1})$ and $\beta = \sin^{-1}(v_{n2}/V)$, where $V = [v_{n1}^2 + v_{n2}^2 + v_{n3}^2]^{1/2}$. The relationships are linearized by applying assumption 2:

$$ V \cong v_{n1}, \qquad \alpha \cong v_{n3}/V, \qquad \beta \cong v_{n2}/V \tag{28} $$

Next, Eqs. (28) are differentiated to produce

$$ \dot{V} \cong F_{n1}/m_s, \qquad \dot{\alpha} \cong (\dot{v}_{n3}/V) - (\alpha F_{n1}/m_s V) \qquad \dot{\beta} \cong (\dot{v}_{n2}/V) - (\beta F_{n1}/m_s V) \tag{29} $$

and complex notation is used to produce a more compact formulation for the AOA and angle of sideslip, and the body rates

$$ \bar{\zeta} = \beta + i\alpha = \frac{v_{n2} + iv_{n3}}{V} \tag{30} $$

$$ \frac{\dot{v}_{n2} + i\dot{v}_{n3}}{V} = \dot{\beta} + i\dot{\alpha} + \frac{F_{n1}}{m_s V}(\beta + i\alpha) \tag{31} $$

and

$$ \bar{\Omega} = \omega_{INn2} + i\omega_{INn3} \tag{32} $$

Equations (24–27) are written in complex notation as

$$ F_{n2} + iF_{n3} = m_s[(\dot{v}_{n2} + i\dot{v}_{n3}) - iv_{n1}(\omega_{INn2} + i\omega_{INn3})] + m_B\dot{\phi}(\dot{p}_{n3} - i\dot{p}_{n2}) $$

$$ M'_{n2} + iM'_{n3} = I'(\dot{\omega}_{INn2} + \dot{\omega}_{INn3}) - iI_{xx}\dot{\phi}(\omega_{INn2} + \omega_{INn3}) - \mu m_B p_{n1}(\ddot{p}_{n3} - i\ddot{p}_{n2}) $$

Upon substitution of Eqs. (30–32), one obtains

$$ \frac{F_{n2} + iF_{n3}}{m_s V} = \dot{\bar{\zeta}} + \frac{F_{n1}}{m_s V}\bar{\zeta} - i\bar{\Omega} + K_3(\dot{p}_{n3} - i\dot{p}_{n2}) \tag{33} $$

$$ \frac{M'_{n2} + iM'_{n3}}{I'} = \dot{\bar{\Omega}} - iK_1\bar{\Omega} - K_2(\ddot{p}_{n3} - i\ddot{p}_{n2}) \tag{34} $$

where

$$ K_1 = (I_{xx}/I')\dot{\phi}, \qquad K_2 = (\mu m_B/I')p_{n1}, \qquad K_3 = m_B\dot{\phi}/m_s V $$

The next step is to specify the form of the aerodynamic forces and moments of Eqs. (33) and (34) in terms of $\bar{\zeta}$, $\bar{\Omega}$, and their time derivatives. By applying assumption 6, the aerodynamic forces and moments are defined as

$$ F_{n1} = -qSC_A, \qquad F_{n2} = qS\left(C_{y_0} + C_{y_\beta}\beta\right) \qquad F_{n3} = qS\left(C_{z_0} + C_{z_\alpha}\alpha\right) $$

$$ T_{n2} = qSd\left[C_{m_0} + C_{m_\alpha}\alpha + C_{m_{\dot{\alpha}}}\left(\frac{\dot{\alpha}d}{2V}\right) + C_{m_{\omega_{INn2}}}\left(\frac{\omega_{INn2}d}{2V}\right) + C_{m_{\dot{\phi}\beta}}\beta\left(\frac{\dot{\phi}d}{2V}\right)\right] $$

$$ T_{n3} = qSd\left[C_{n_0} + C_{n_\beta}\beta + C_{n_{\dot{\beta}}}\left(\frac{\dot{\beta}d}{2V}\right) + C_{n_{\omega_{INn3}}}\left(\frac{\omega_{INn3}d}{2V}\right) + C_{n_{\dot{\phi}\alpha}}\alpha\left(\frac{\dot{\phi}d}{2V}\right)\right] $$

where $q = \frac{1}{2}\rho V^2$, ρ is the atmospheric density, S is the cross-sectional area, d is the reference length, and the zero-subscripted terms account for small aerodynamic asymmetries. These aerodynamic forces and moments can be simplified by applying the aerodynamic symmetry assumption to obtain

$$C_{y_\beta} = C_{z_\alpha} = -C_{N_\alpha}, \qquad C_{n_\beta} = -C_{m_\alpha}, \qquad C_{n_{\dot\beta}} = -C_{m_{\dot\alpha}}$$
$$C_{n_{\omega_{IN}n3}} = C_{m_{\omega_{IN}n3}}, \qquad C_{n_{\dot\phi\alpha}} = C_{m_{\dot\phi\beta}}$$

The left-hand sides of Eqs. (33) and (34) can now be evaluated by substituting the definitions just given:

$$F_{n2} + iF_{n3} = qS\left[C_{y_0} + iC_{z_0} - C_{N_\alpha}\bar\zeta\right] \tag{35}$$

$$\begin{aligned} M'_{n_2} + iM'_{n_3} &= qS\left[d\left(C_{m_0} + iC_{n_0}\right) + \mu p_{n_1}\left(C_{z_0} - iC_{y_0}\right)\right. \\ &+ \mu C_A\left(p_{n_3} - ip_{n_2}\right) + i\left(\mu p_{n_1} C_{N_\alpha} - C_{m_\alpha} d\right)\bar\zeta \\ &+ C_{m_{\omega_{IN}n2}}(d^2/2V)\bar\Omega - iC_{m_{\dot\alpha}}(d^2/2V)\dot{\bar\zeta} \\ &\left.+ C_{m_{\dot\phi\beta}}(\dot\phi d^2/2V)\bar\zeta\right] \end{aligned} \tag{36}$$

Equations (33) and (35) can be algebraically manipulated to give a relationship between $\bar\Omega$ and $\bar\zeta$:

$$\begin{aligned} \bar\Omega &= -i\dot{\bar\zeta} + i(qS/m_s V)\left[C_A - C_{N_\alpha}\right]\bar\zeta \\ &+ i(qS/m_s V)\left[C_{y_0} + iC_{z_0}\right] - K_3(\dot p_{n2} + i\dot p_{n3}) \end{aligned} \tag{37}$$

The substitution of Eq. (37) and its first derivative, along with Eq. (36), into Eq. (34) produces the desired linear, time-varying autopilot equation

$$\ddot{\bar\zeta} + \bar A\dot{\bar\zeta} + \bar B\bar\zeta = \bar C \tag{38}$$

where

$$\begin{aligned} \bar A &= -\left[(qS/m_s V)\left(C_A - C_{N_\alpha}\right)\right. \\ &\left.+ (qSd^2/2VI')\left(C_{m_{\dot\alpha}} + C_{m_{\omega_{IN}n2}}\right) + iK_1\right] \end{aligned}$$

$$\begin{aligned} \bar B &= -\left[\frac{\dot q S}{m_s V}\left(C_A - C_{N_\alpha}\right) + \left(\frac{qSC_A}{m_s V}\right)^2\left(1 - \frac{C_{N_\alpha}}{C_A}\right)\right. \\ &- \left(\frac{qSd}{V}\right)^2\left(\frac{C_{m_{\omega_{IN}n2}}}{2m_s I'}\right)\left(C_A - C_{N_\alpha}\right) + \frac{qS}{I'}\left(C_{m_\alpha} d - C_{N_\alpha}\mu p_{n1}\right) \\ &\left.+ i\left(\frac{-qSK_1}{m_s V}\left[C_A - C_{N_\alpha}\right] + \frac{qSd^2}{2VI'}\dot\phi C_{m_{\dot\phi\beta}}\right)\right] \end{aligned}$$

$$\begin{aligned} \bar C &= \left(C_{y_0} + iC_{z_0}\right)\left[\left(\frac{\dot q S}{m_s V}\right) + \left(\frac{qS}{m_s V}\right)^2 C_A\right. \\ &\left.- \left(\frac{qSd}{V}\right)^2\left(\frac{C_{m_{\omega_{IN}n2}}}{2m_s I'}\right) - i\frac{qS}{m_s V}K_1\right] - \frac{qSd}{I'}\left(C_{n_0} - iC_{m_0}\right) \\ &+ \frac{qS}{I'}\mu p_{n1}\left(C_{y_0} + iC_{z_0}\right) + \frac{qS}{I'}\mu C_A(p_{n2} + ip_{n3}) \\ &+ [K_1K_3 + i\dot K_3](\dot p_{n2} + i\dot p_{n3}) + [K_2 + iK_3](\ddot p_{n2} + i\ddot p_{n3}) \end{aligned}$$

and the nonrolling mass position is defined in terms of the body-fixed mass position as

$$\boldsymbol{p}^N = \begin{pmatrix} 0 \\ p_2\cos\phi - p_3\sin\phi \\ p_2\sin\phi + p_3\cos\phi \end{pmatrix} \tag{39}$$

The last step is to justify the assumption that $\ddot\phi$ is small. By linearizing the nonrolling roll rate equation, the following relationship is derived:

$$\begin{aligned} \ddot\phi &= (1/I_{xx})[T_{n1} + \mu(p_{n3}F_{n2} - p_{n2}F_{n3})] \\ &= (qS/I_{xx})\left[C_{l_0}d + C_{l_{\dot\phi}}(\dot\phi d^2/2V)\right. \\ &\left.+ \mu\left(C_{y_0}p_{n3} - C_{z_0}p_{n2}\right)\right] \end{aligned} \tag{40}$$

which demonstrates that $\ddot\phi$ is small for small aerodynamic asymmetries and roll torques.

Evaluation of Autopilot Equations

The goal of this section is to derive a set of theoretical design tools for choosing and sizing MMTC systems. The first step is to solve Eq. (38) for the steady-state complex AOA. If one considers a slender vehicle ($I' \gg I_{xx}$) that flies along a constant flight-path angle through an exponential atmosphere, then the $\bar B$ term reduces to

$$\begin{aligned} \bar B &= -qS\left\{(1/I')\left(C_{m_\alpha}d - C_{N_\alpha}\mu p_{n1}\right)\right. \\ &\left.+ i\left[(K_1/m_s V)\left(C_A - C_{N_\alpha}\right) + (d^2/2VI')\dot\phi C_{m_{\dot\phi\beta}}\right]\right\} \end{aligned}$$

and neglecting aerodynamic asymmetries, the $\bar C$ term becomes

$$\bar C = \bar C_1 + \bar C_2$$

where

$$\bar C_1 = (qS/I')\mu C_A(p_{n2} + ip_{n3})$$

and

$$\bar C_2 = [K_1K_3 + i\dot K_3](\dot p_{n2} + i\dot p_{n3}) + [K_2 + iK_3](\ddot p_{n2} + i\ddot p_{n3})$$

The steady-state complex AOA is

$$\bar\zeta_T = \bar C/\bar B = \bar\zeta_{T_1} + \bar\zeta_{T_2} = (\bar C_1/\bar B) + (\bar C_2/\bar B) \tag{41}$$

where $\bar\zeta_{T_1}$ is the trim angle contribution resulting from the center of mass offset and $\bar\zeta_{T_2}$ is the contribution due to PAM. The major contribution of $\bar\zeta_{T_1}$ to $\bar\zeta_T$ is defined by setting the body-fixed roll rate to zero ($\dot\phi = 0$) and assuming the mass is not moving in the body-fixed frame to obtain

$$\bar\zeta_{T_1} = \frac{-\mu C_A(p_{n2} + ip_{n3})}{\left(C_{m_\alpha}d - C_{N_\alpha}\mu p_{n1}\right)} = \beta_{T_1} + i\alpha_{T_1} \tag{42}$$

The major contribution of $\bar\zeta_{T_2}$ to $\bar\zeta_T$ is difficult to evaluate in the nonrolling frame, but can be determined in the body-fixed frame. The limiting trim angle is given by Hodapp and Clark[7] and is equal to the PAM angle:

$$\left|\zeta_{T_2}\right| \cong \frac{m_P p_{n1}}{I'} p_{n23} \tag{43}$$

where p_{n23} is the largest radial displacement of the moving mass. As a result, one can expect to obtain an AOA that is approximately equal to the PAM angle if the moving mass can be manipulated properly. The proper manipulation of the mass will be described in the next section.

The theoretical design tools, or rules of thumb, are Eqs. (42) and (43). Equation (42) is used to size an MMTC for slow spinning ballistic vehicles that have small SM (SM < 10% of body length), whereas Eq. (43) is employed for fast spinning vehicles that have SMs greater than 10% of body length. The dividing line between slow and fast spinning is the critical roll rate,[7]

$$\omega_{cr} = \left[\frac{-C_{m_\alpha}qSd}{I' - I_{xx}}\right]^{\frac{1}{2}} \tag{44}$$

This dividing line determines the dominance of either aerodynamic or inertial forces and moments. The aerodynamic forces dominate when the body-fixed roll rate is below ω_{cr}, whereas the inertial forces dominate when the roll rate is above ω_{cr}. Consequently, one is designing an MMTC that is either a trim due to drag system (subcritical) or a trim due to PAM system (supercritical).

Performance Examples

The first step in sizing an MMTC is to perform 3-DOF trajectory simulations of the ballistic vehicle to determine the required trim AOA for a given divert capability. The results of 3-DOF simulations for a sphere–cone RV and a rocket are presented in Figs. 2 and 3. The divert capability for an RV is strongly influenced by the flight-path angle and the divert initiation altitude. The steeper trajectories require more AOA for the same divert capability, and there is an upper divert initiation altitude limit at approximately 90 kft. The results of the rocket simulations show the tradeoff between downrange and cross-range performance. Given these relationships between divert capability and AOA, one can employ the rules of thumb of the previous section to design MMTCs for ballistic vehicles.

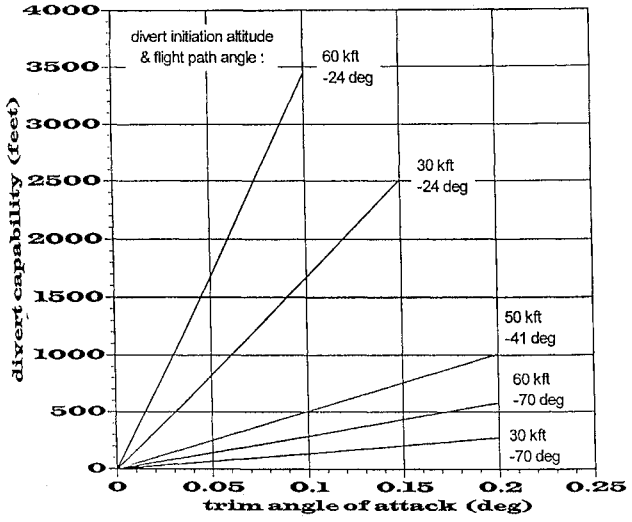

Fig. 2 RV divert capability for various initial conditions.

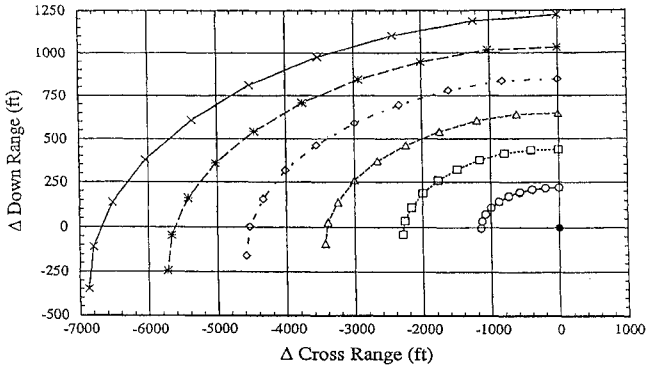

Fig. 3 Rocket divert capability for various trim angles. Rocket impacts for various trim conditions. •, α_{Trim} = 0.00 deg; ○, α_{Trim} = 0.05 deg; □, α_{Trim} = 0.10 deg; △, α_{Trim} = 0.15 deg; ◇, α_{Trim} = 0.20 deg; ✳, α_{Trim} = 0.25 deg; and ×, α_{Trim} = 0.30 deg.

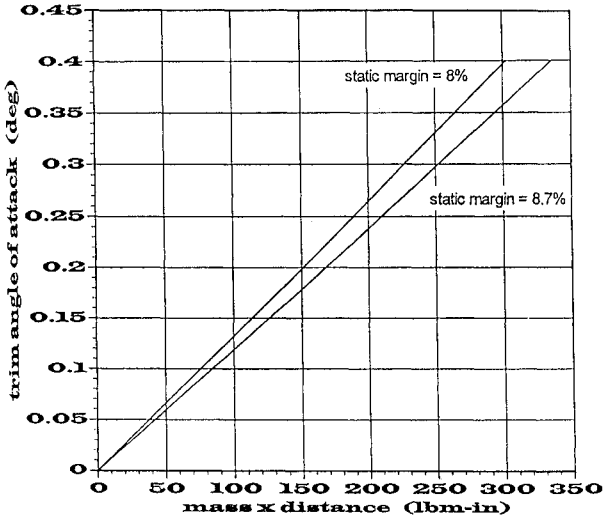

Fig. 4 RV static trim angle capability.

Subcritical Control (RV)

As stated earlier, the subcritical control example is a sphere–cone RV with a base diameter of 22 in., a nose radius of 2 in., a total length of 62 in., and a total mass of 400 lbm. Equation (42) is used to calculate the approximate relationship between the steady-state trim AOA and the required mass moment. The results are displayed in Fig. 4. The required mass moment is a linear function of the AOA, and the slope of the line becomes steeper as the SM is decreased. For this example, the desired divert capability is 1150 ft, which corresponds to a trim AOA of 0.22 deg for a flight-path angle of −41 deg and a divert initiation altitude of 50 kft, a mass moment of 170 lbm-in., and an SM of 8%. The MMTC was designed with a maximum radial stroke of 7 in. and a 24-lbm moving mass (i.e., a mass ratio of 6%). The 8-DOF simulation results of the RV MMTC with a simple open-loop autopilot that holds the moving mass fixed in the nonrolling frame in the cross-range direction are presented in Figs. 5–7. Figure 5 confirms that the MMTC delivers the desired cross-range divert with minimal downrange change. Figure 6 verifies the desired trim AOA performance. Figure 7 shows that the roll rate performance is stable.

Three conceptual layouts for the RV MMTC are presented in Fig. 8 with an allowable cylindrical volume of 17 in. diam by 8

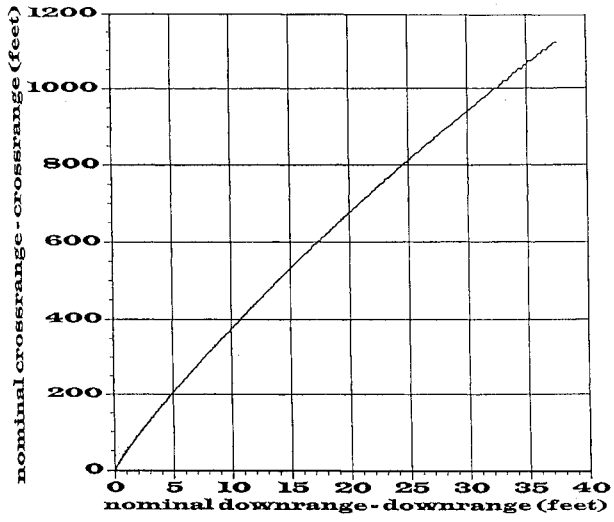

Fig. 5 RV cross-range divert.

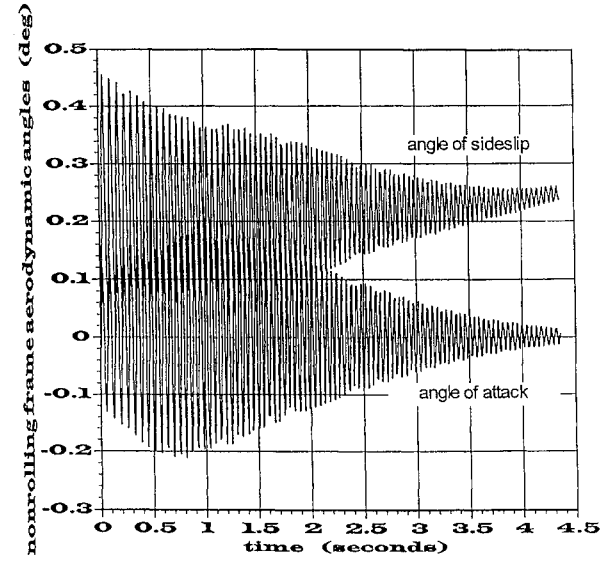

Fig. 6 RV AOA and angle of sideslip.

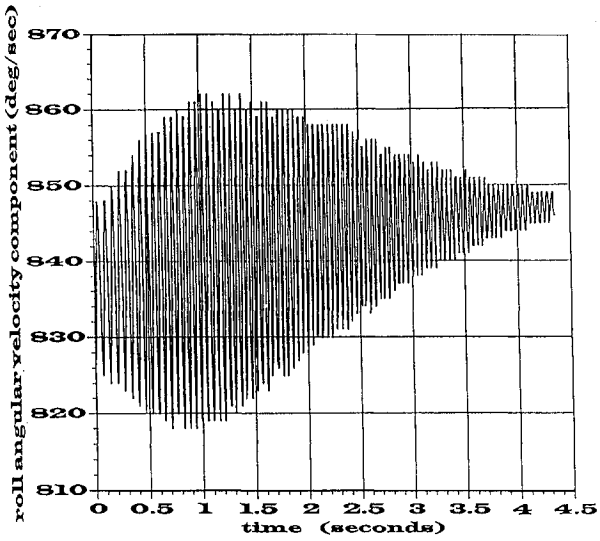

Fig. 7 RV body-fixed roll rate.

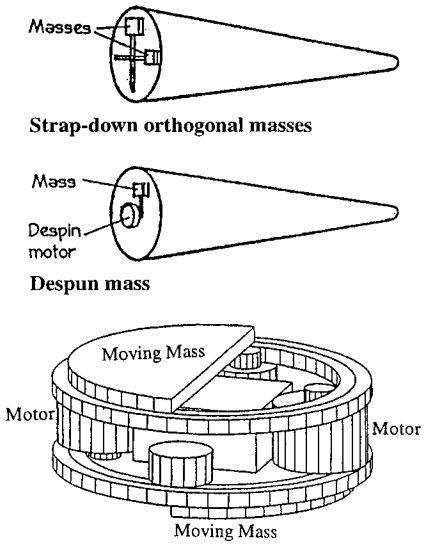

Fig. 8 Three RV moving mass layouts.

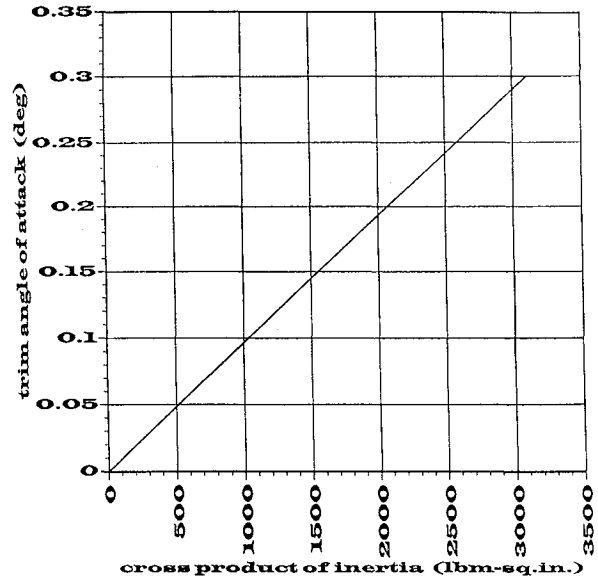

Fig. 9 Rocket trim angle capability with PAM.

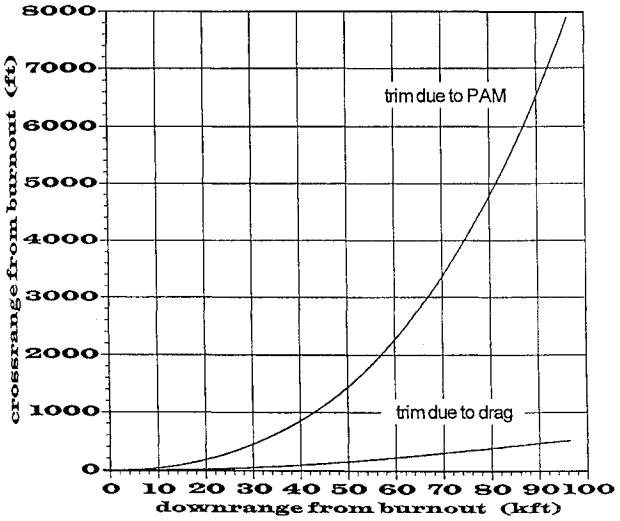

Fig. 10 Rocket cross-range divert.

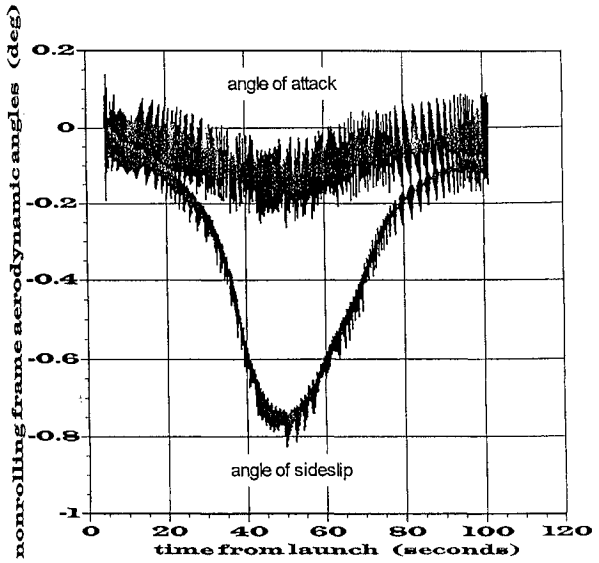

Fig. 11 Rocket AOA and angle of sideslip.

in. length. The first and third layouts require two moving masses, whereas the second uses a single mass. The approximate layout for a given RV depends on the application.

Supercritical Control (Rocket)

The supercritical performance example is a fast spinning rocket that is described in Ref. 8. The important dimensions of this rocket are a mass of 670 lbm, a 9 in. diam, and a 13 ft length. Equation (43) is used to calculate the approximate relationship between the trim AOA and the required PAM. The results for a sea level flight are presented in Fig. 9. Since the rocket is flying through a varying atmosphere (from 0 to 40,000 ft), the sizing of the mass must be iterated upon using the simulation. For this example, the desired divert capability is 8000 ft, which corresponds to a trim AOA of 0.35 for control after burnout to impact. This required trim AOA is an average value over the trajectory, and the peak AOA is approximately an order of magnitude larger than the value given by Eq. (43).

The MMTC was designed with a maximum stroke of 4 in. and a 5-lbm moving mass, which produces a cross product of inertia equal to 1200 lb-in.^{2}. The simulation results of the rocket MMTC are displayed in Figs. 10–12. Figure 10 confirms that the PAM MMTC provides the desired cross-range divert, whereas the trim resulting from drag MMTC produces nearly zero divert. Figure 11 shows that the AOA and sideslip angle performance match the prediction of Eq. (43) at low altitudes near launch and impact (AOA $\cong$ 0.1 deg) and follow the dynamic pressure profile and the altitude history

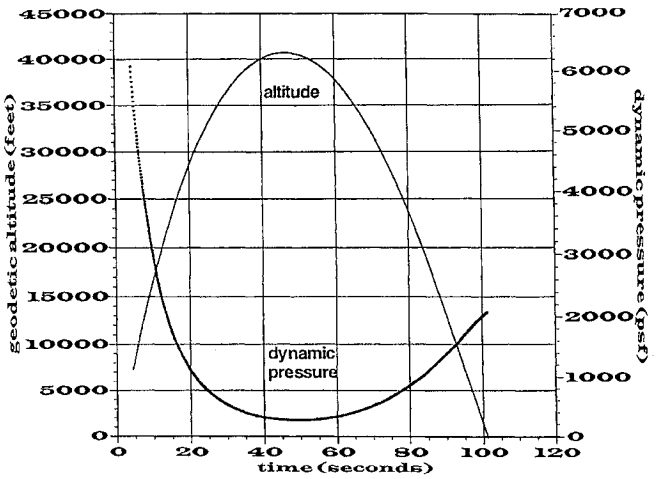

Fig. 12 Rocket altitude and dynamic pressure.

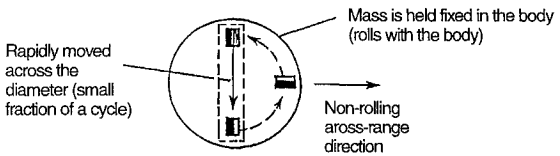

Fig. 13 Rocket moving mass articulation and actuator layout.

(Fig. 12). The autopilot system in this MMTC simulation is more complicated than the RV MMTC because one is attempting to create inertial forces due to PAM in a nonrolling frame. This is a problem because the inertial forces rely on the roll rate squared, and the nonrolling roll rate is approximately zero. The way to overcome this problem is to articulate the mass in the body-fixed frame such that the mass is held fixed over a portion of the cycle in the desired direction. The motion of the mass is presented in Fig. 13. This cyclic motion accounts for the cyclic variation of the AOA. This open-loop autopilot can be characterized as a bang–bang type of control system where the AOA is controlled by the number of times the mass is actuated in a given direction. The conceptual layout is a relatively simple one as most bang–bang actuators are in practical applications. It amounts to a single mass that slides in a piston tube behind the warhead section. The allowable volume is a cylinder that is 8 in. in diameter and 11 in. long. The mass ratio of the MMTC is 5/670, or 0.7%.

Conclusions

The focus of this work was to assess the feasibility of MMTCs to increase the accuracy of axisymmetric, ballistic vehicles. A general set of equations of motion for a single moving mass was derived in the body-fixed and nonrolling frames. These equations of motion were linearized and manipulated to produce a general set of autopilot equations that relate the motion of the moving mass in the body-fixed frame to the AOA and sideslip angle in the nonrolling frame. These autopilot equations can be used to develop closed-loop control systems for the MMTCs.

The assessment began by evaluating the effectiveness of aerodynamic vs inertial forces for different vehicles. A set of rules of thumb were developed that categorize the ballistic vehicles of interest. Basically, fast spinning vehicles were shown to use trim due to PAM because the body-fixed roll rate is above the critical roll rate and the inertial forces are dominant. The slow spinning vehicles employ trim resulting from drag since the roll rate is subcritical and the aerodynamic forces are dominant. One important point to keep in mind when dealing with slow spinners is that the SM must be sufficiently small (less than 10%) to produce a reasonably sized MMTC.

These design rules of thumb were verified by simulating MMTCs for a sphere–cone RV and a rocket. The RV MMTC performed as predicted by the design rules, whereas the rocket MMTC predictions were low because the design rules assumed a constant atmosphere and a constant flight-path angle. However, during each interval that these assumptions were valid, the predictions were accurate.

Finally, conceptual designs were presented that demonstrated the feasibility of MMTCs, for our simulation models given reasonable physical constraints. The MMTCs fit within the allowable volume and weighed only a few percent of the vehicle's total weight for these examples. Although these example cases demonstrated the feasibility of MMTCs, the most important aspect of this paper is the presentation of general design and analysis tools that can be used to evaluate prospective ballistic vehicles and MMTCs.

Acknowledgment

This work was supported by the U.S. Department of Energy under Contract DE-AC04-76DP00789.

References

[1]Regan, F. J., *Re-Entry Vehicle Dynamics*, AIAA Education Series, AIAA, New York, 1984.

[2]Nelson, R. L., Price, D. A., and Delpino, F. H., "New Concept for Controlled Lifting Entry Flight Experiments," LMSC-677802, NASA CR 66718, April 1967.

[3]Petsopoulos, T., and Regan, F. J., "A Moving-Mass Roll Control System for a Fixed-Trim Reentry Vehicle," AIAA Paper 94-0033, Jan. 1994.

[4]Regan, F. J., and Kavetsky, R. A., "Add-On Controller for Ballistic Reentry Vehicles," Patent, Serial No. 752,766, U.S. Dept. of Commerce, Washington, DC, 1984.

[5]White, J. E., and Robinett, R. D., III, "Principal Axis Misalignment Control for Deconing of Spinning Spacecraft," *Journal of Guidance, Control, and Dynamics*, Vol. 17, No. 4, 1994, pp. 823–830.

[6]Kane, T. R., and Levinson, D. A., *Dynamics: Theory and Applications*, McGraw–Hill, New York, 1985.

[7]Hodapp, A. E., Jr., and Clark, E. L., Jr., "A Technique for Determining Approximate Roll Rate Histories for Ballistic Reentry Vehicles Having Mass, Inertia, and Aerodynamic Asymmetries," Sandia National Labs., Rept. SC-RR-69-804, Albuquerque, NM, Sept. 1970.

[8]Dohrmann, C. R., Eisler, G. R., and Robinett, R. D., "Dynamic Programming Approach for Burnout-To-Apogee Guidance of Precision Munitions," *Journal of Guidance, Control, and Dynamics*, Vol. 19, No. 2, 1996, pp. 340–346.